



A two-stage adaptive multi-fidelity surrogate model-assisted multi-objective genetic algorithm for computationally expensive problems

Qi Zhou¹ · Jinhong Wu¹ · Tao Xue¹ · Peng Jin¹

Received: 17 May 2019 / Accepted: 8 August 2019 / Published online: 20 August 2019
© Springer-Verlag London Ltd., part of Springer Nature 2019

Abstract

Surrogate model-assisted multi-objective genetic algorithms (MOGA) show great potential in solving engineering design problems since they can save computational cost by reducing the calls of expensive simulations. In this paper, a two-stage adaptive multi-fidelity surrogate (MFS) model-assisted MOGA (AMFS-MOGA) is developed to further relieve their computational burden. In the warm-up stage, a preliminary Pareto frontier is obtained relying only on the data from the low-fidelity (LF) model. In the second stage, an initial MFS model is constructed based on the data from both LF and high-fidelity (HF) models at the samples, which are selected from the preliminary Pareto set according to the crowding distance in the objective space. Then the fitness values of individuals are evaluated using the MFS model, which is adaptively updated according to two developed strategies, an individual-based updating strategy and a generation-based updating strategy. The former considers the prediction uncertainty from the MFS model, while the latter takes the discrete degree of the population into consideration. The effectiveness and merits of the proposed AMFS-MOGA approach are illustrated using three benchmark tests and the design optimization of a stiffened cylindrical shell. The comparisons between the proposed AMFS-MOGA approach and some existing approaches considering the quality of the obtained Pareto frontiers and computational efficiency are made. The results show that the proposed AMFS-MOGA method can obtain Pareto frontiers comparable to that obtained by the MOGA with HF model, while significantly reducing the number of evaluations of the expensive HF model.

Keywords Multi-fidelity surrogate model · Model management · Prediction uncertainty · Simulation-based design · Optimization

1 Introduction

Practical engineering design optimization problems usually contain several objectives, in which at least two of them are conflicting in nature. Therefore, solving these problems generally results in multiple optimal solutions termed as Pareto-optimal solutions. Multi-objective genetic algorithms (MOGAs) have been widely used for obtaining these Pareto-optimal solutions, due to its advantages including ease of implementation, no need of the gradient information of the objective functions or constraints, and great ability

to handle problems with nonconvex Pareto fronts. Despite these advantages, it is still impractical for them to solve engineering problems that involve time-consuming simulations. This is because MOGAs usually require a large number of fitness evaluations to locate near-optimal solutions. A promising way to improve the efficiency of such algorithms is to incorporate the surrogate model, also referred as the metamodel or approximation model, in evolutionary computations for reducing the computationally expensive exact fitness evaluations [1, 2]. The incorporations of surrogate models, e.g., Gaussian process (GP) model [3], neural network (NN) [4], radial basis function (RBF) [5, 6], could be achieved in almost all elements of the evolutionary computations, which can be classified into three types [7]. The first incorporation strategy is termed as surrogate model-assisted migration, in which individuals approximated with different levels of accuracy can migrate from one subpopulation to another. The second one is termed as

✉ Peng Jin
pengjin_hust@hust.edu.cn

¹ School of Aerospace Engineering, Huazhong University of Science and Technology, Wuhan 430074, People's Republic of China

surrogate model-assisted initialization and genetic operations [8]. Since initialization, crossover, and mutation are usually implemented randomly, it is believed that using the surrogate model for initializing the populations and guiding the crossover and mutation would be beneficial for accelerating the convergence rate. The last one is termed as surrogate model-assisted fitness evaluations, in which the surrogate model is constructed to replace the time-consuming simulations aiming at reducing the number of fitness calculations [9–11]. Since the surrogate model-assisted fitness evaluations can lead to the best performance among the above three strategies, there has been widespread interests in these approaches [12–15].

The surrogate model-assisted fitness evaluation approaches can be broken down into two distinct modes, off-line (non-adaptive) mode and on-line (adaptive) mode [16–21]. In the off-line mode, a pre-specified amount of sample points are employed to build a surrogate model, which is used for the fitness evaluations in the evolutionary computation subsequently. The main shortcoming of the off-line mode is that it is difficult to predetermine the proper sample size for obtaining an accurate surrogate model, which will lead to the reduction of the number of fitness evaluations not be significant [22]. On the other hand, the on-line mode generates an initial surrogate model first and then adaptively updates the surrogate model following some model management strategies during the evolutionary computation. Compared with the off-line mode, the on-line mode can make use of the knowledge from previous iterations and is reported to be more efficient for evolutionary algorithms [23]. The core factor that determines the success of on-line surrogate model-assisted fitness evaluations is the model management strategy, i.e., to update the surrogate model in the evolutionary computation, which individuals should be selected to be evaluated using the exact fitness functions. The most straightforward idea is to evaluate the individuals that are potentially with the best fitness values, the largest degree of prediction uncertainty, maximum space-filling characteristic, or individuals that can make a trade-off between the fitness values and surrogate model accuracy. Randomly selecting individuals to evaluate with the real fitness function in each generation for updating the surrogate model was also studied. Preliminary efforts have demonstrated that these management strategies with a pre-defined updating number may cause oscillation because the prediction accuracy of the surrogate model may vary significantly during optimization. To address this issue, Li et al. [8] proposed an effective kriging surrogate model-assisted MOGA, in which an objective measure is developed to select the individuals whose dominated states will be changed because of the prediction error from the surrogate model. Furthermore, Li [17] improved this method by introducing an enhanced quantitative switching criterion.

Although the previous work demonstrated the obvious merits of surrogate-assisted MOGAs, for the computationally expensive high-fidelity (HF) models, even performing the number of simulations needed for constructing a surrogate model could be too expensive [24–32]. To further alleviate the high computational cost in HF analyses, an efficient alternative termed as the multi-fidelity surrogate (MFS) modeling is recognized recently. In MFS, an assumption is made that there exists a low-fidelity (LF) model, which is less accurate compared with the corresponding HF model but is considerably less computationally demanding [33–36]. By integrating the information from both LF and HF models, i.e., the LF model is used to provide the trend of the quantity of interests (QoI), whereas a small number of HF simulations are used to guarantee the prediction accuracy in the critical subspaces, MFS can make a trade-off between high accuracy and low computational expense [28, 37–40]. The most notable of MFS is the cokriging surrogate model developed by Kennedy and O’Hagan [41], where a Bayesian method was proposed for predicting the responses of the HF model with the assistance of several LF models. Han et al. [36] developed an extended cokriging surrogate model in which the cokriging weights were refined and a scaling factor was introduced to consider the effects of LF data on the prediction of the HF model. Furthermore, Zhou et al. [42] developed an uncertainty quantification approach to concurrent treat the effects of uncertainties from design variables and MFS in the robust optimization. Nguyen et al. [43] combined the MFS with the multidisciplinary feasible approach to ease the computational burden caused by the high-fidelity analysis in multidisciplinary design optimization (MDO).

Though MFS has been reported as being used in engineering design, its combination with the multi-objective evolutionary algorithms is scarce. When the computational cost of the LF model should be taken into consideration, Shu et al. [44] proposed an on-line MFS-assisted MOGA, which can decide whether the LF model or the HF model would be selected to analyze for a sample point, recently, while in the case of that the computational cost of the LF model can be ignored compared with the HF model, Liu et al. [45] combined the MFS with MOGA, in which the MFS was constructed based on the multiplicative scaling function, and successfully applied it to light-weight design of a stiffened panel. However, the prediction uncertainty introduced by the MFS, which can have a significant effect on the accuracy of the obtained Pareto set, was ignored in this approach [46]. Therefore, in this work, a two-stage adaptive MFS-assisted MOGA (AMFS-MOGA) is developed to improve the accuracy for combining the MFS with MOGA. In the warm-up stage, a preliminary Pareto set is obtained relying only on the data from the LF model. In the second stage, an initial MFS is constructed based on the data from both LF and HF

models at the samples, which are selected from the preliminary Pareto set according to the crowding distance in the objective space. Then the fitness values of individual are evaluated by the MFS, which is adaptively updated according to two developed strategies, individual-based updating strategy and generation-based updating strategy. The former considers the prediction uncertainty from the MFS, while the latter takes the discrete degree of the populations into consideration. The performance of the proposed AMFS-MOGA approach is illustrated using three benchmark test functions and the design optimization of the hull of an autonomous underwater vehicle. The comparisons between the proposed AMFS-MOGA approach and some existing approaches considering the quality of the obtained Pareto frontiers and computational efficiency are made. The merits of AMFS-MOGA approach are analyzed and summarized.

The remainder of this paper is organized as follows. In Sect. 2, the background and terminology of the multi-objective optimization and multi-fidelity surrogate model are presented. Details of the proposed AMFS-MOGA are introduced in Sect. 3. In Sect. 4, the comparison results between the proposed approach and some existing approaches on three benchmark test functions and a real-world engineering design problem are presented. In Sect. 5, the concluding remarks and possible future work are given.

2 Background and terminology

2.1 Multi-objective optimization problems (MOPs)

Generally, MOPs can be formulated as,

$$\begin{aligned} & \text{minimize } F(\mathbf{x}) = \{f_1(\mathbf{x}), f_2(\mathbf{x}), \dots, f_m(\mathbf{x})\} \\ & \text{subject to } g_j(\mathbf{x}) \leq 0, \quad j = 1, 2, \dots, J \\ & \mathbf{x}_{lb} \leq \mathbf{x} \leq \mathbf{x}_{ub}, \end{aligned} \quad (1)$$

where $F(\mathbf{x})$ denotes the objective function vector, m denotes the number of objective functions, \mathbf{x} denotes the design variable vector with the lower and upper bounds are \mathbf{x}_{lb} and \mathbf{x}_{ub} , respectively. $g_j(\mathbf{x})$ is the j th constraint. Since at least two of the objective functions are conflicting, therefore, solving Eq. (1) generally results in multiple optimal solutions termed as Pareto-optimal solutions. The objective function values at these Pareto-optimal solutions form the Pareto frontier. A large number of MOGAs can be used to obtain the Pareto frontier for global optimization. Particularly, a modified non-dominated sorting in genetic algorithms (NSGA-II) proposed by Deb et al. [47] is used in this work.

2.2 Multi-fidelity surrogate model

The motivation of MFS modeling is that many cheaper LF sampling points are adopted to reduce the computational cost while a limited number of expensive HF sampling points are used to ensure the prediction accuracy of the surrogate model. Noted that this motivation is based on the assumption that the LF model can provide a general trend of the QOI. Three common ways to obtain a LF model are [33, 46, 48]: (a) simplifying the analysis model (e.g., by using a coarse finite element mesh instead of a refined mesh); (b) simplifying the modeling concept or domain [e.g., by using a two-dimensional (2D) model instead of a three-dimensional (3D) one], and (c) simplifying the mathematical or physical description (e.g., by using the Euler non-cohesive equations instead of the Navier–Stokes viscous Newton equations). It should be noted that the LF and HF models are a relative concept. Take an airfoil design, which is an aerodynamic component, as an example. For obtaining the aerodynamic coefficients, when compared with the 2D computational fluid dynamic (CFD) simulation with Euler non-cohesive equations, a 3D CFD simulation with Navier–Stokes viscous Newton equations could be termed as HF model, whereas it would be treated as LF model when the wind tunnel experiments are available.

Generally, the MFS based on the interaction of the HF model and the LF model can be expressed as [49],

$$\hat{F}(\mathbf{x}, \mathbf{a}) \equiv \hat{F}(f^l(\mathbf{x}), \mathbf{a}) \approx F(\mathbf{x}), \quad (2)$$

where \mathbf{x} is the design vector, $\hat{F}(\mathbf{x}, \mathbf{a})$ denotes the MFS that is used to replace the actual HF model, $f^l(\mathbf{x})$ represents the response of the LF model, $F(\mathbf{x})$ represents the actual response of the HF surrogate model, and \mathbf{a} is a vector of tuning parameters used for minimizing the discrepancy between the LF and HF models. From the above definition, the MFS $\hat{F}(\mathbf{x}, \mathbf{a})$ tends to approach the high accuracy of the HF model, but at a considerably less computational effort.

3 The proposed approach

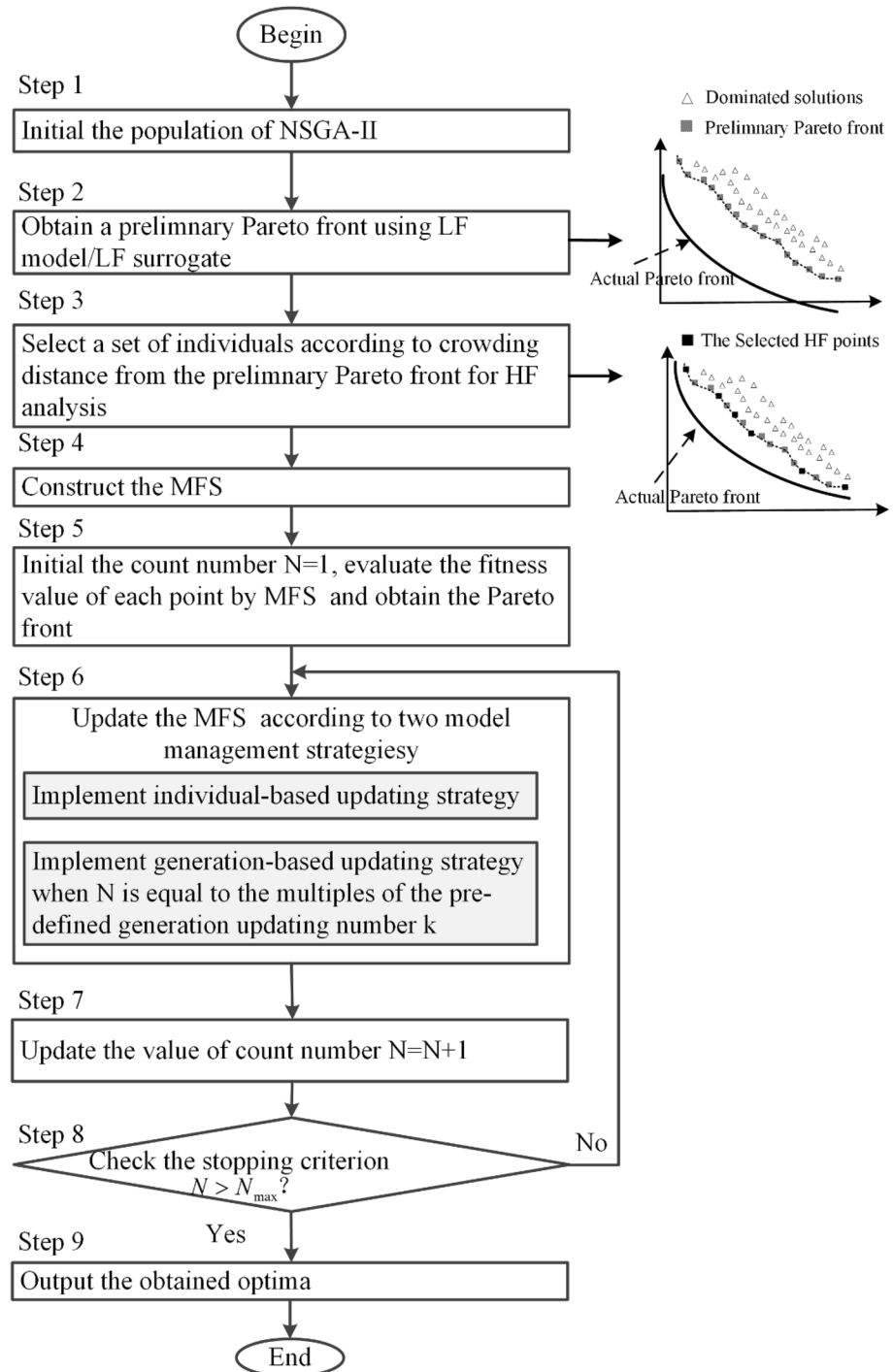
The goal of the proposed AMFS-MOGA approach is to improve the efficiency of the MOGA by adopting a two-stage adaptive MFS approach. In the warm-up stage, a preliminary Pareto front is obtained by the LF model or LF surrogate model. In the second stage, a set of individuals from the preliminary Pareto front are selected to be simulated by the HF model. Then, these HF sample data are fused with the LF model or LF surrogate model for constructing the MFS model. The preliminary Pareto set is re-evaluated as the initial individuals and the MFS model is used for the fitness evaluations in the second stage to

obtain the final Pareto front. During the evolutionary process, two model management strategies, individual-based updating strategy and generation-based updating strategy, are developed to improve the efficiency and convergence of the proposed approach further. In the following subsections, we present the core ideas of AMFS-MOGA approach as two parts. They are (1) multi-fidelity surrogate model approach and (2) model management strategies. The flowchart for the proposed method is plotted in Fig. 1.

3.1 Multi-fidelity surrogate model approach

Commonly used MFS approaches are scaling methods, in which the MFS is obtained by tuning the LF model using scaling function according to the responses of the HF model [37, 50]. In this work, the MFS approach proposed in our previous work [51] is adopted, where the LF model or a tuned LF surrogate model is taken as a base model and is

Fig. 1 The flowchart of the proposed method



mapped to the studied HF model using a kriging surrogate model. For completeness, a brief review of this MFS approach is presented here. A more detailed description can be found in Ref. [51]. In the MFS approach, if the relationships between the input variables and corresponding responses could be expressed explicitly in the LF model, the model will be directly used without the need of constructing a surrogate model. Otherwise, a LF surrogate model needs to be built, e.g., using kriging, for MFS. To tune the LF surrogate model and make it as close to the HF model as possible, an optimization procedure can be taken as,

$$\min : L(a_0, a_1) = \sum_{i=1}^m [(a_0 + a_1 \hat{f}^l(x_i^h)) - f^h(x_i^h)]^2 \tag{3}$$

$$\text{s.t. } l_0 \leq a_0 \leq u_0, l_1 \leq a_1 \leq u_1,$$

where $L(a_0, a_1)$ represents the loss function in the least-square-error sense and x_i^h is the i th sample point of the HF model. The bounds posed on tuning parameters represent the prior knowledge of the global constant bias and multiplicative scaling between LF and HF models, respectively.

Once the LF model or tuned LF surrogate model is obtained, the scaling process is implemented as follows. For a given HF sample set $\mathbf{x}^h = \{x_1^h, x_2^h, \dots, x_{m_h}^h\}$ with m_h HF sample points and the corresponding responses $\mathbf{f}^h = \{f_1^h, f_2^h, \dots, f_{m_h}^h\}$, the discrepancies $\mathbf{C}(\mathbf{x}) = \{c(x_1^h), c(x_2^h), \dots, c(x_{m_h}^h)\}$ between the HF and LF model/surrogate model for a HF sample point x_i^h can be calculated as,

$$\begin{cases} c(x_i^h) = f^h(x_i^h) - f^l(x_i^h) & \text{(if LF model is used)} \\ c(x_i^h) = f^h(x_i^h) - a_0^* - a_1^* \hat{f}^l(x_i^h) & \text{(if LF surrogate is used)} \end{cases} \tag{4}$$

where $f^h(x_i^h)$ is the actual response of the HF model at x_i^h , $f^l(x_i^h)$ is the real response of the LF model for x_i^h , and $\hat{f}^l(x_i^h)$ is the predicted value of the LF surrogate model for x_i^h .

Based on the HF sample set $\mathbf{x}^h = \{x_1^h, x_2^h, \dots, x_{m_h}^h\}$ and corresponding discrepancy or scaling data $\mathbf{C}(\mathbf{x}) = \{c(x_1^h), c(x_2^h), \dots, c(x_{m_h}^h)\}$, the scaling function $\mathbf{C}(\mathbf{x})$ modeled using the kriging can be expressed as,

$$\begin{cases} \hat{\mathbf{C}}(\mathbf{x}) = \hat{\beta}_h + (\mathbf{r}_h)^T (\mathbf{R}_h)^{-1} (\mathbf{f}^h(\mathbf{x}) - \mathbf{f}^l(\mathbf{x}) - \hat{\beta}_h \mathbf{p}) \\ \hat{\beta}_h = (\mathbf{p}^T \mathbf{R}_h^{-1} \mathbf{p})^{-1} \mathbf{p}^T \mathbf{R}_h^{-1} (\mathbf{f}^h(\mathbf{x}) - \mathbf{f}^l(\mathbf{x})) \end{cases} \text{(if LF model is used)} \tag{5}$$

$$\begin{cases} \hat{\mathbf{C}}(\mathbf{x}) = \hat{\beta}_h + (\mathbf{r}_h)^T (\mathbf{R}_h)^{-1} (\mathbf{f}^h(\mathbf{x}) - (a_0^* + a_1^* \hat{\mathbf{f}}^l(\mathbf{x})) - \hat{\beta}_h \mathbf{p}) \\ \hat{\beta}_h = (\mathbf{p}^T \mathbf{R}_h^{-1} \mathbf{p})^{-1} \mathbf{p}^T \mathbf{R}_h^{-1} (\mathbf{f}^h(\mathbf{x}) - (a_0^* + a_1^* \hat{\mathbf{f}}^l(\mathbf{x}))) \end{cases} \text{(if LF surrogate is used),}$$

where $\mathbf{r}_h \in R^{m_h}$ and $\mathbf{R}_h \in R^{m_h}$ denote the correlation vector and correlation matrix, respectively, and \mathbf{p} is a column vector of length m_h that is filled with ones.

After the LF model or LF surrogate model and the scaling function are constructed, the MFS that is used to approximate the HF model can be expressed as,

$$\begin{cases} \hat{\mathbf{f}}_{\text{vf}}(\mathbf{x}) = \mathbf{f}^l(\mathbf{x}) + \hat{\mathbf{C}}(\mathbf{x}) & \text{(if LF model is used)} \\ \hat{\mathbf{f}}_{\text{vf}}(\mathbf{x}) = a_0^* + a_1^* \hat{\mathbf{f}}^l(\mathbf{x}) + \hat{\mathbf{C}}(\mathbf{x}) & \text{(if LF surrogate is used)} \end{cases} \tag{6}$$

3.2 Model management strategies

Model management strategies have a significant impact on the success of the surrogate model-based MOGA methods. The core of the model management strategy is to identify which sample points should be selected from the current population to improve the prediction accuracy of the surrogate model. In the proposed AMFS-MOGA, two model management strategies are adopted. One is an individual-based updating strategy aiming to take the interpolation uncertainty from MFS model into consideration, and the other one is a generation-based updating strategy aiming to improve the degrees of the dispersion of the populations. In the following subsections, these two strategies are described in more details.

3.2.1 Individual-based updating strategy

The predicted fitness values of the individuals from the MFS model have prediction uncertainty, which may mislead the evolutionary process. Therefore, an individual-based updating strategy is developed to take the interpolation uncertainty of the MFS model into consideration. As mentioned, although this work focuses on the case that the computational cost of the LF model can be ignored compared with the HF model, the LF model or the LF surrogate model would be used in the MFS. This will lead to two different types of uncertainty quantifications of the interpolation uncertainty from the MFS. On the one hand, when the LF model is directly used in the MFS, the interpolation uncertainty of the MFS only comes from the scaling function $\hat{\mathbf{C}}(\mathbf{x})$. The predicted variance of the scaling function $\hat{\mathbf{C}}(\mathbf{x})$ can be calculated as,

$$\sigma_c^2(x_o) = \hat{\sigma}_c^2 \left[1 - (\mathbf{r}_c)^T (\mathbf{R}_c)^{-1} \mathbf{r}_c + \frac{(1 - \mathbf{p}^T (\mathbf{R}_c)^{-1} \mathbf{r}_c)^2}{\mathbf{p}^T (\mathbf{R}_c)^{-1} \mathbf{p}} \right] \tag{7}$$

Therefore, the prediction interval $I(x_o)$ for an individual x_o from the MFS can be modeled as an interval with 95.5% confidence level. Then the bounds of the prediction interval $I_{95.5\%}(x_o)$ are two times the standard deviation ($2\sigma_c(x_o)$) from each side of the mean.

On the other hand, when the LF surrogate model is used, the predicted variance of the MFS is quantified by calculating the sums of the predicted variance of the two surrogate models, one for the LF surrogate model $\hat{f}^l(x)$ and the other for the scaling function $\hat{C}(x)$. It can be calculated by

$$\sigma_{\text{mfs}}^2(x_o) = (a_1^*)^2 \sigma_1^2(x_o) + \sigma_c^2(x_o), \tag{8}$$

where $\sigma_1^2(x_o)$ is predicted variance of LF surrogate model. It can be calculated by

$$\sigma_1^2(x_o) = \hat{\sigma}_1^2 \left[1 - (r_1)^T (R_1)^{-1} r_1 + \frac{(1 - p^T (R_1)^{-1} r_1)^2}{p^T (R_1)^{-1} p} \right]. \tag{9}$$

Note that as long as the domination status of the individual may not change due to the interpolation uncertainty of the MFS model, its fitness value can be predicted by the MFS model instead of expensive simulation models. However, if the domination status of the individual may change, then its fitness value should be evaluated by simulation models. In this work, the objective switching criterion [52] that relates the minimum of minimum distance (MMD) and the prediction interval is extended to MFS scenarios to determine whether the simulation models or the MFS model should be used to evaluate the fitness of individuals. In each generation, the MMD, which is used to measure the lower bound of the distance between the points in dominated and non-dominated set, is calculated. The illustration of the calculation process for MMD is presented in Fig. 2. In Fig. 2, the distance between two points, e.g., $d(A, a)$, is calculated by the Euclidean distance.

The different relationships between the MMD and prediction interval can result in two different scenarios of the individuals. For simplicity, the illustrations of the types of individuals on one-dimensional of the objective space are presented in Figs. 3 and 4, respectively.

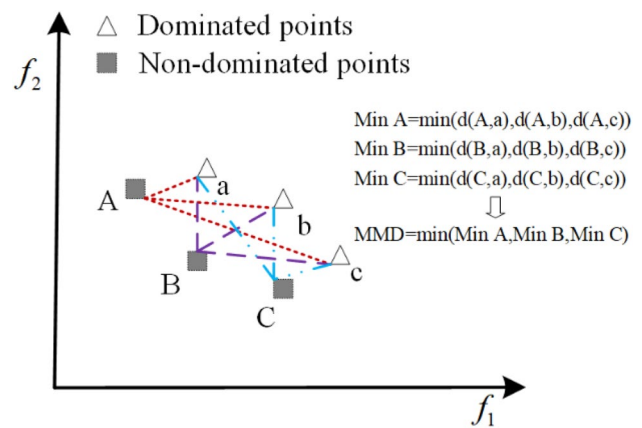


Fig. 2 The illustration of the calculation process for MMD

As can be seen in Figs. 3a and 4a, no matter how the individuals “A” and “a”, move within the corresponding prediction interval $I_{95.5\%}(A)$ and $I_{95.5\%}(a)$, the individual “a” always dominated by the individual “A”. It means that for these scenarios although the MFS model has interpolation uncertainty at individuals, “A” and “a”, these interpolation uncertainties do not affect the domination status of these two individuals at the given confidence probability. Therefore, it is no need to add these individuals as new sample points for updating the MFS model in the subsequent evolutionary process. On the contrary, as seen in Figs. 3b and 4b, the probability interval of the non-dominated individual “A” overlaps with that of the dominated individual “a”. It means that the domination status of the individual “A” would be changed because of the interpolation uncertainty from the MFS model. Then these two individuals, “A” and “a”, should be sent to HF analysis to avoid the misleading of the searching. In summary, the individuals that satisfy the following condition will be sent for HF analysis,

$$\frac{1}{2}I_{95.5\%}(A) + \frac{1}{2}I_{95.5\%}(a) \geq \text{MMD}(f_1), \tag{10}$$

where

$$\begin{cases} \frac{1}{2}I_{95.5\%}(A) = 2\sigma_c(A); \frac{1}{2}I_{95.5\%}(a) = 2\sigma_c(a) & (\text{if LF model is used}) \\ \frac{1}{2}I_{95.5\%}(A) = 2\sigma_{\text{mfs}}(A); \frac{1}{2}I_{95.5\%}(a) = 2\sigma_{\text{mfs}}(a) & (\text{if LF surrogate is used}) \end{cases} \tag{11}$$

Fig. 3 Two scenarios for the individuals when the LF model is used

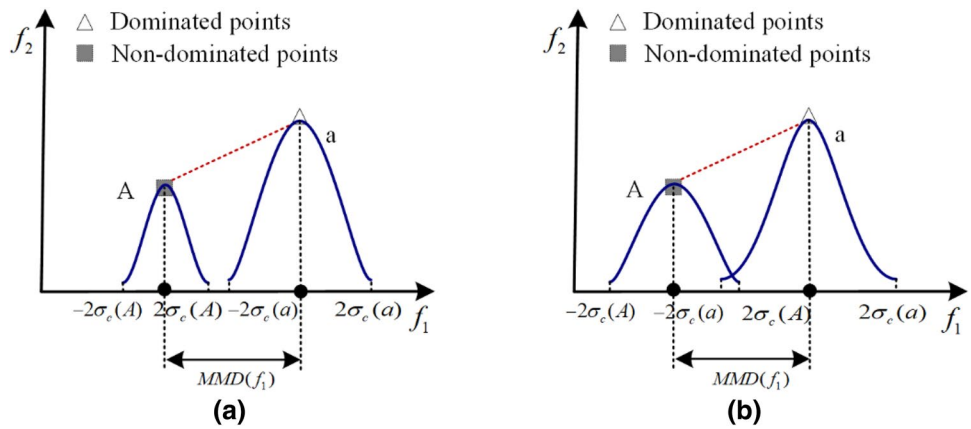


Fig. 4 Two scenarios for the individuals when LF surrogate model is used

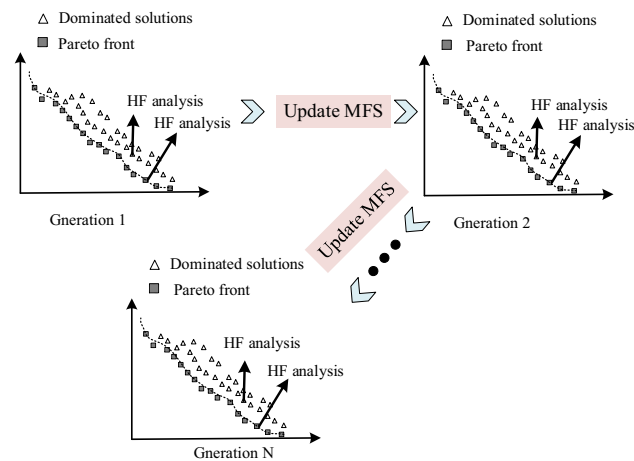
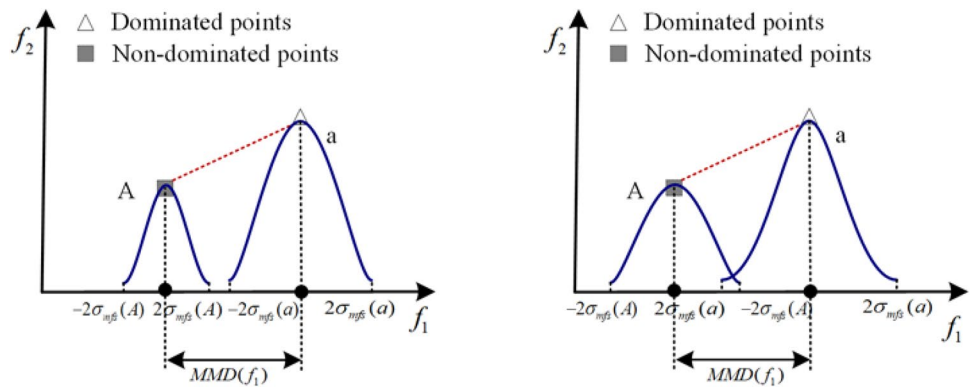


Fig. 5 The schematic plot of the individual-based updating strategy

Figure 5 depicts the schematic of this developed individual-based updating strategy. Notice that the MFS will be updated after each generation by adding the individuals according to the developed individual-based updating strategy. Table 1 provides the algorithm of the developed individual-based updating strategy.

3.2.2 Generation-based updating strategy

The uniformity of the Pareto set maybe not good if the solution is updated only according to the above individual-based updating strategy. To improve the diversity of the Pareto set, a generation-based updating strategy is developed, in which the point with the maximum degree of diversity is selected for HF analysis after a fixed number of generations. These points can be obtained by solving the following equation

$$\text{Find : } x$$

$$\text{Max} = \min_{1 \leq m \leq l} (d(x, x_m^0)) \quad x_m^0 \in X_{P_m}, \tag{12}$$

where $d(x, x_m^0)$ is defined to be the Euclidean distance between x and the m th training point in the current HF sampling set X_{P_m} .

Figure 6 depicts a schematic of the developed generation-based updating strategy. The algorithm for selecting such individuals is listed in Table 2.

Table 1 The algorithm of individual-based updating strategy

Algorithm 1. Individual-based updating strategy.	
Input: The individuals in the current generation.	
1	Begin
2	$\{x_A, x_B, \dots\}_{\text{non-dominated}}, \{x_a, x_b, \dots\}_{\text{dominated}}$ ← Obtain the non-dominated and dominated points
	$MMD = \min \{\ f(p) - f(q)\ _2\}$ ← Calculate the MMD between non-dominated and dominated points.
3	$p = x_A, x_B, \dots$ $q = x_a, x_b, \dots$ ← Obtain $MMD(f_m)$ by objecting MMD along the objective function axis
4	$MMD(f_m)$ ← Calculate the prediction intervals of the points
5	$I_p(x_A), I_p(x_B), \dots, I_p(x_a), I_p(x_b), \dots$ ← Sort the individuals based on prediction interval values in descending order.
6	$I_p(x_1) \geq I_p(x_2) \geq \dots \geq I_p(x_n) \geq 0$
7	For $i=1$ to n do
8	if $I_p(x_i) + I_p(x_{i+1}) > 2MMD_{f_i}$
9	HF(x_i) ← x_i is sent for HF analysis.
10	else
11	break for
12	end if
13	end for
Output: $\{x_1, x_2, \dots, x_j\}$	

Fig. 6 The schematic plot of the generation-based updating strategy

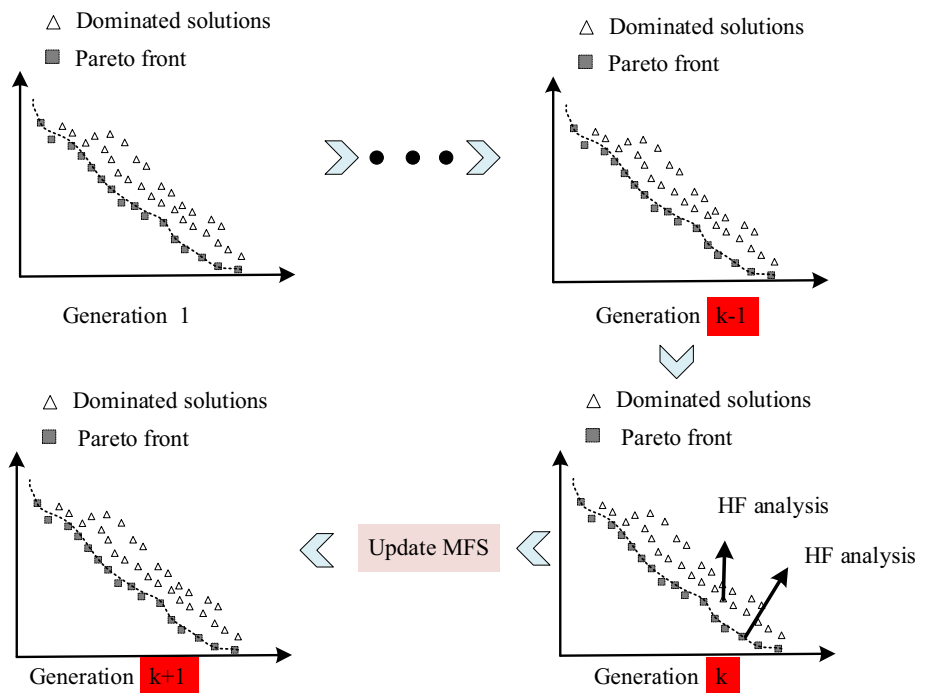


Table 2 The algorithm of generation-based updating strategy

Algorithm 2. Generation-based updating strategy.	
Input: The existing HF evaluated point set $X_p = \{x_{p_1}, x_{p_2}, \dots, x_{p_l}\}$, the current generation number i , the pre-defined density and the max-number of generation-based updating generations update.	
1	Begin
2	if $i/10 == 0$ & $i \leq \text{update}$ do
3	for $j = 1$ to <i>density</i>
4	$Max = \min_{1 \leq m \leq l} (d(x, x_m^0)) \quad x_m^0 \in X_{p_m}$ \leftarrow Obtain the j^{th} point.
5	$X_p = \{x_{p_1}, x_{p_2}, \dots, x_{p_l}, x_j\}$ \leftarrow Add the j^{th} point to the HF sampling set.
6	$l = l + 1$ \leftarrow Update the number of points in X_p
7	end for
8	end if
Output: $\{x_1, x_2, \dots, x_{\text{density}}\}$	

3.3 Steps for the proposed AMFS-MOGA approach

As a supplement to the flowchart of the proposed approach depicted in Fig. 1, detailed steps of the proposed approach are presented as follows:

Stage I

- Step 1: Initialize the population of NSGA-II.
- Step 2: Obtain a preliminary Pareto frontier by NSGA-II, in which the fitness values for each individual are evaluated by the LF model or LF surrogate model.

Stage II

- Step 3: Select a set of individuals that have the same number of the offset from the preliminary Pareto frontier based on crowding distance in the objective space. Then, these individuals are sent to the HF model for analysis.
- Step 4: Construct the MFS according to the approach described in Sect. 3.1.
- Step 5: Initialize the count number $N = 1$, evaluate the fitness values for individual by using the constructed MFS and obtain the Pareto front by NSGA-II.
- Step 6: Update the MFS by the two model management strategies described in Sect. 3.2. Notice that the generation-based updating strategy is implemented when the current generation number is equal to multiples of the pre-defined generation updating number k .
- Step 7: Update the count number $N = N + 1$.

- Step 8: Check whether the stopping criterion is satisfied. If yes, go to Step 9; otherwise, go back to Step 6.
- Step 9: Output the obtained Pareto set.

4 Examples and results

4.1 Numerical examples

In this section, three well-used numerical benchmarks (ZDT1, ZDT2, and ZDT3) with different degrees of complexity are used to illustrate the applicability and efficiency of the proposed AMFS-MOGA approach. In these three numerical examples, the original mathematical functions [53], described in Eqs. (7)–(9), are taken as the HF models. The LF models are assumed to be the Taylor expansion of the HF models. To test the applicability of the proposed approach for different situations, it is assumed that a LF surrogate model needs to be constructed in the ZDT3, while for ZDT1 and ZDT2, the LF models can be directly used for the MFS without fitting a surrogate model to replace them. The settings in the NSGA-II for these benchmarks are given in Table 3.

Table 3 The settings of NSGA-II in the numerical benchmarks

Parameter	ZTD1	ZTD2	ZTD3
Population size	100	100	100
No. generations	200	200	200
Offset	30	30	30
Update	100	100	100
Density	5	5	10

ZDT1

$$\text{minimize } f_1(x) = x_1$$

$$f_2(x) = g(x) \times h(x)$$

$$\text{where } g(x) = 1 + \frac{9}{n-1} \sum_{i=2}^n x_i \quad (13)$$

$$h(x) = 1 - \sqrt{f_1(x)/g(x)}$$

$$n = 3$$

$$0 \leq x_i \leq 1, i = 1, \dots, n.$$

ZDT2

$$\text{minimize } f_1(x) = x_1$$

$$f_2(x) = g(x) \times h(x)$$

$$\text{where } g(x) = 1 + \frac{9}{n-1} \sum_{i=2}^n x_i \quad (14)$$

$$h(x) = 1 - (f_1(x)/g(x))^2$$

$$n = 3$$

$$0 \leq x_i \leq 1, i = 1, \dots, n.$$

ZDT3

$$\text{minimize } f_1(x) = x_1$$

$$f_2(x) = g(x) \times h(x)$$

$$\text{where } g(x) = 1 + \frac{9}{n-1} \sum_{i=2}^n x_i \quad (15)$$

$$h(x) = 1 - \sqrt{f_1(x)/g(x)} - (f_1(x)/g(x)) \sin(10\pi f_1)$$

$$n = 3$$

$$0 \leq x_i \leq 1, i = 1, \dots, n.$$

4.2 Quality metrics

To compare the ability of obtaining desirable Pareto frontiers and the efficiency of different approaches, two metrics for measuring the quality of Pareto frontiers [54, 55], i.e., the relative hyperarea difference (RHD) and overall spread (OS), and the HF function calls (FC) for measuring the efficiency

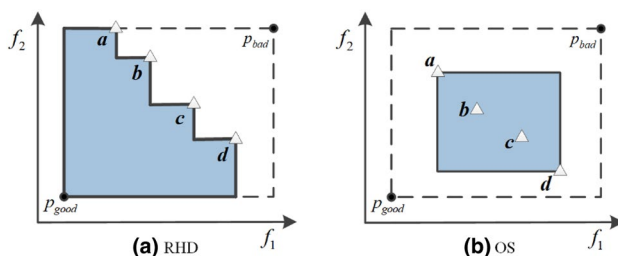


Fig. 7 Quality metrics **a** RHD and **b** OS [46]

of different approaches, are calculated. The RHD and OS represent the convergence and diversity of the obtained Pareto frontier, respectively. The smaller the value of RHD is, the higher convergence of the Pareto frontier would be, while a larger value of OS indicates a more diverse Pareto frontier.

Figure 7 illustrates these two metrics geometrically for a 2D case. Let the current Pareto set to be $P = \{a, b, c, d\}$. p_{good} and p_{bad} are the extreme “good” and “bad” points, respectively. The quantity RHD, shown as in Fig. 7a, is defined as the relative difference between the area bounded by p_{good} and p_{bad} , and the shaded area covered from p_{bad} to the current robust Pareto set P . The quantity OS, shown as in Fig. 7b, is defined as the ratio between the area bounded by two extreme points a and d in the current robust Pareto set P and the area bounded by p_{good} and p_{bad} .

4.3 Results and comparisons

For comparison, four other methods are considered: (1) MOGA with LF model (2) MOGA with HF model (3) kriging surrogate model-assisted MOGA (K-MOGA) proposed by Li et al. [52], and (4) Multiplication-scale multi-fidelity surrogate model-assisted MOGA (MMFS-MOGA) proposed by Zhu et al. [56]. For each approach, 15 runs are conducted for all examples to account for the influence of randomness. Figure 8 demonstrates the typical Pareto frontiers obtained from one of the 15 runs of these approaches.

As illustrated in Fig. 8, the Pareto frontiers from the three surrogate model-assisted MOGA, i.e., K-MOGA, MMFS-MOGA, and AMFS-MOGA, are consistent with that of the MOGA with HF model, while only a small portion of the Pareto frontier of MOGA with LF model overlap with those from the MOGA with HF model. This indicates that it is difficult to obtain the true Pareto frontier by only incorporating the LF model into the MOGA. It is worth to mention that compared with K-MOGA and MMFS-MOGA, the proposed AMFS-MOGA does not lose the boundary points that on the Pareto frontier of the MOGA with HF model. This is attributed to the developed generation-based updating strategy in the AMFS-MOGA, which is very helpful for improving the degree of dispersion of the populations.

To further demonstrate the superiority of the proposed approach, the quality of convergence, diversity of Pareto optimum, and the computational efforts for the MOGA with HF model are summarized in Table 4. The comparison results of the proposed AMFS-MOGA, K-MOGA and MMFS-MOGA are summarized in Table 5. In Table 5, “FC” denotes the required HF function calls. Notice that one function call in Tables 4 and 5 refer to the calculation of objective and constraints together for a single individual.

As illustrated in Tables 4 and 5, the average values of RHD and OS from the K-MOGA, MMFS-MOGA, and

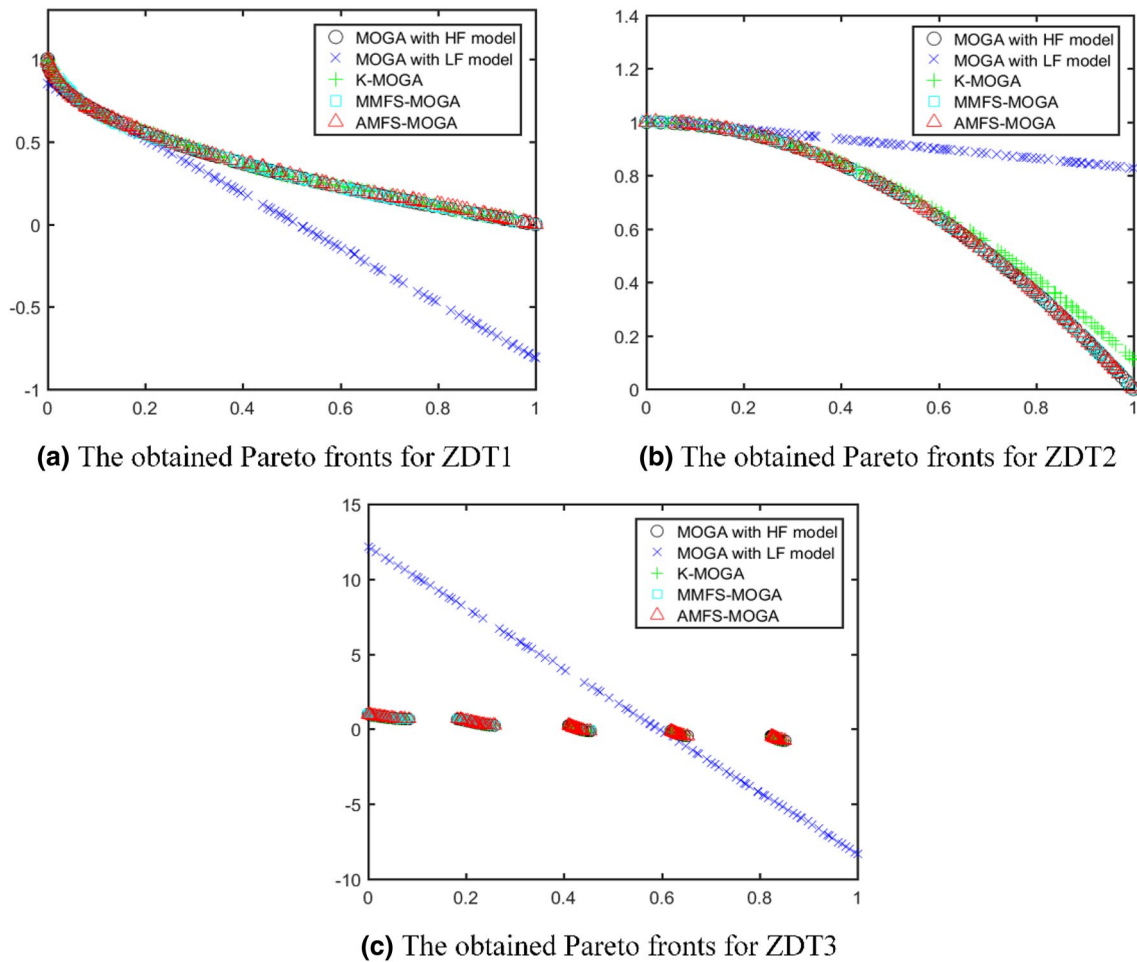


Fig. 8 The obtained Pareto frontiers for numerical cases using different approaches

Table 4 Quantity metrics of the NSGA-II with HF model for numerical cases

Cases	Metrics	NSGA-II with HF model		
		15 runs	Mean	STD
ZDT1	RHD	[0.2686 0.2693]	0.269	1.72E-04
	OS	[0.5102 0.5102]	0.5102	1.15E-16
	FC	[19,047 19,146]	19,092	27.431
ZDT2	RHD	[0.4388 0.4394]	0.439	1.41E-04
	OS	[0.5102 0.5102]	0.5102	1.15E-16
	FC	[19,032 19,141]	19,092	32.4345
ZDT3	RHD	[0.1362 0.1371]	0.1364	2.09E-04
	OS	[0.7693 0.7707]	0.7706	3.61E-04
	FC	[19,015 19,151]	19,105	33.6695

AMFS-MOGA are close to those of the MOGA with HF model in all numerical examples. This means that these three surrogate model-assisted MOGA approaches can obtain a comparable convergence and diversity of Pareto

sets compared with the MOGA with HF model. Another observation is that considering the standard deviation (STD) values in RHD and OS, K-MOGA and MMFS-MOGA perform worse than the proposed AMFS-MOGA approach.

Regarding the computational efficiency of these four approaches, the number of function calls for AMFS-MOGA is nearly 100 times less than that of the MOGA with HF model. Meanwhile, the average number of function calls is reduced by 45–60% using the AMFS-MOGA compared to that of the K-MOGA. Compared to MMFS-MOGA, the average number of function calls is reduced by 30% for ZDT1 and ZDT2. Figure 9 demonstrates the HF function calls for ZDT2 in all the 15 runs for each approach. As illustrated in Fig. 9, the proposed AMFS-MOGA run with the number of HF calls (the maximum of 160) requires 100 times fewer than that of the MOGA with HF model run (the minimum of 1.9×10^4). All individuals will be evaluated by the HF model for obtaining their fitness values in the MOGA with HF model, whereas only a small portion of them are needed to be analyzed using the HF model in

Table 5 Comparison of different approaches for numerical cases

Cases	Metrics	K-MOGA			MMFS-MOGA			AMFS-MOGA		
		15 runs	Mean	STD	15 runs	Mean	STD	15 runs	Mean	STD
ZDT1	RHD	[0.2263 0.3645]	0.2708	0.0311	[0.2022 0.2671]	0.2507	0.0187	[0.2490 0.2703]	0.2594	0.006
	OS	[0.2416 0.8533]	0.5498	0.1593	[0.2134 0.6025]	0.4117	0.1108	[0.3046 0.5049]	0.4797	0.0497
	FC	[109 470]	343.33	90.87	190	190	0	[88 248]	135	51.3471
ZDT2	RHD	[0.4356 0.5083]	0.4471	0.0176	[0.4387 0.4392]	0.4390	0.0002	[0.4384 0.4393]	0.439	2.48E-04
	OS	[0.2220 0.5307]	0.4668	0.0725	[0.5102 0.5102]	0.5102	0	[0.5068 0.5012]	0.5098	8.77E-04
	FC	[185 406]	279.2	76.2104	190	190	0	[103 166]	131.8	17.5467
ZDT3	RHD	[0.1250 0.1889]	0.1423	0.0174	[0.1084 0.1318]	0.1263	0.0064	[0.1015 0.1307]	0.1308	0.0088
	OS	[0.4771 0.8566]	0.7729	0.0879	[0.1329 0.5614]	0.1886	0.1039	[0.7199 0.8987]	0.7828	0.0414
	FC	[248 745]	466	143.35	222	222	0	[130 367]	221.26	64.659

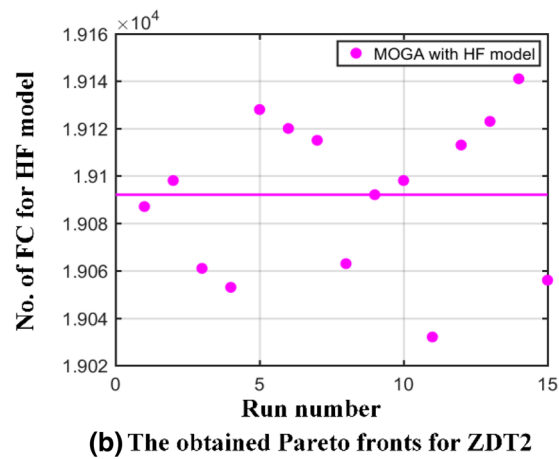
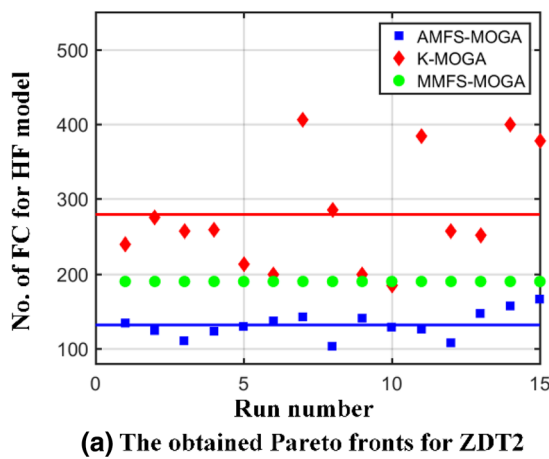


Fig. 9 No. of HF function evaluations versus run number for ZDT2

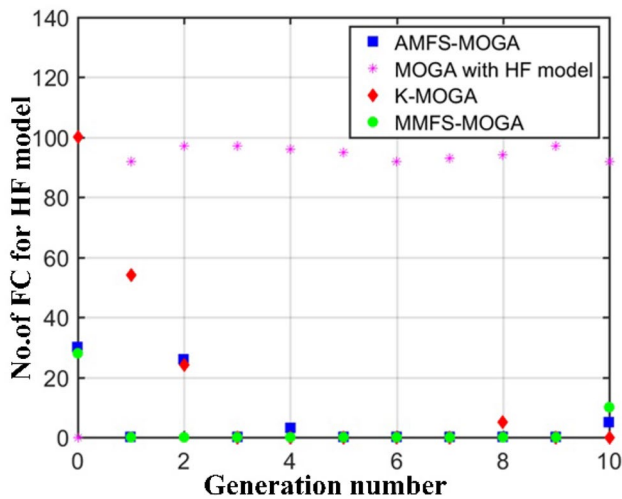


Fig. 10 No. of HF function evaluations in the early evolution process for ZDT2

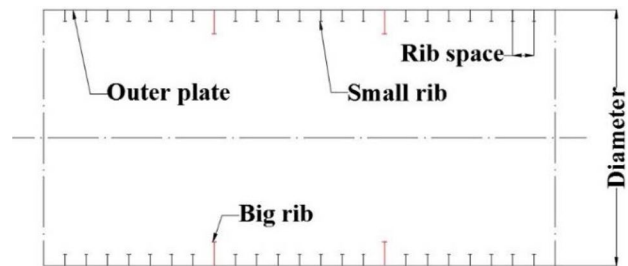


Fig. 11 The structural profile of the stiffened cylindrical shell with variable ribs

AMFS-MOGA. It is worth to mention that although there is no need for the K-MOGA and MMFS-MOGA to analyze all individuals by HF model in the evolution process, it still requires a larger number of function calls than that

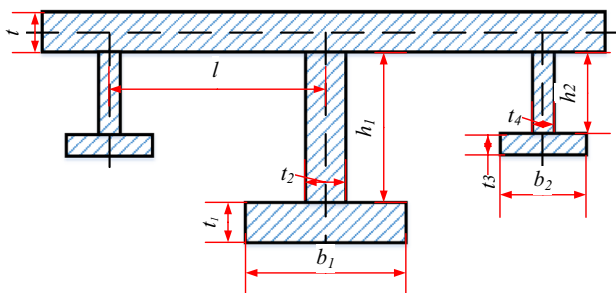


Fig. 12 The schematic plot of the stiffened cylindrical shell

of AMFS-MOGA. This is because the proposed AMFS-MOGA can not only make full use of the uncertainty information from MFS but also the data from both LF and HF models for updating MFS.

Figure 10 depicts the number of function calls for the HF model in the first fifteen generations at one of the 15 runs for different approaches. As can be seen in Fig. 10, K-MOGA requires evaluating more individuals with HF model than the proposed AMFS-MOGA to reduce the prediction uncertainty of the surrogate model in the early stage of the evolution process. MMFS-MOGA needs to evaluate more individuals in the later generations. As a result, the total number of function calls for the HF model in the proposed AMFS-MOGA is less than those of K-MOGA and MMFS-MOGA. Noted that although we detail the merits of computational efficiency for AMFS-MOGA in ZDT2, similar results can also be obtained in ZDT1 and ZDT3.

Table 6 Ranges and values of the design variables and parameters

Design variables	Ranges	Values
The thickness of the outer shell t	18–28 mm	–
Large ribs		
The thickness of the webs t_2	12–22 mm	–
The height of the webs h_1	250–300 mm	–
The thickness of the face panels t_1	14–26 mm	–
The width of the face panels b_1	80–120 mm	–
Small ribs		
The thickness of the webs t_4	20–30 mm	–
The height of the webs h_2	450–500 mm	–
The thickness of the face panels t_3	22–35 mm	–
The width of the face panels b_2	130–170 mm	–
Distance between T-ribs l	–	500 mm
The length of the shell L	–	12,000 mm
The radius of the shell R	–	3500 mm
The hydrostatic pressure P_j	–	3 MPa

Table 7 Material properties

Design variables	Values
Elastic modulus E	2.1×10^5 MPa
Density ρ	7850 kg/m ³
Yield limit σ_s	550 MPa
Poisson’s ratio μ	0.3

4.4 Engineering case

In this section, the developed approach is applied to the design optimization for a stiffened cylindrical shell with variable ribs. The structural profile of the stiffened cylindrical shell with variable ribs is shown in Fig. 11. Figure 12 depicts the schematic of the big ribs and small ribs of the cylindrical shell. The object of this problem is to minimize the weight and improve the stability of the stiffened cylindrical under the constraints of relevant regulations. The design variables are the space of ring-ribs l , the sizes of large and small ribs’ webs and face panels. Other parameters are fixed during the optimization process. The ranges and values for these design variables and parameters are depicted in Table 6. The material property is listed in Table 7.

Therefore, the optimization problem can be defined as,

$$\begin{aligned}
 &\text{Minimize } [M, -p_{cr2}] \\
 &\text{Subject to } g_1 = \frac{\sigma_1}{0.85\sigma_s} - 1 \leq 0, \quad g_2 = \frac{\sigma_2}{1.15\sigma_s} - 1 \leq 0, \\
 &g_3 = \frac{\sigma_3}{0.60\sigma_s} - 1 \leq 0, \quad g_4 = 1 - \frac{P_{cr1}}{p_j} \leq 0, \\
 &g_5 = 1 - \frac{p_{cr2}}{1.2p_j} \leq 0, \quad g_6 = \frac{h_1}{23t_2} - 1 \leq 0, \\
 &g_7 = \frac{b_1}{6t_1} - 1 \leq 0, \quad g_8 = \frac{h_2}{23t_4} - 1 \leq 0 \\
 &g_9 = \frac{b_2}{6t_3} - 1 \leq 0,
 \end{aligned}
 \tag{16}$$

where M is the total weight of the stiffened cylindrical shell, σ_1 is mid-plane circumferential stress of the shell, σ_2 donates the longitudinal stress of the outer-face of the shell at rib, σ_3 is the rib stress, P_{cr1} represents the local buckling pressure, P_{cr2} represents the global buckling pressure. Intuitively, as the mass increases, the load required to destabilize the structure increases.

In this work, two-levels of fidelity models, the LF empirical model and HF simulation model, are used to obtain the objective and constraint values.

In the LF empirical model, the $\sigma_1, \sigma_2, \sigma_3, P_{cr1}$ and P_{cr2} can be computed by the following formulas

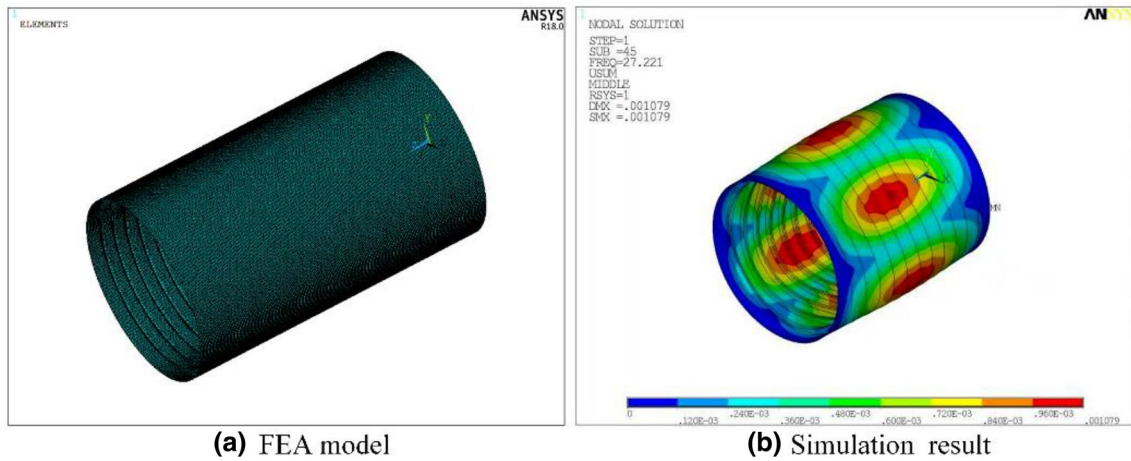


Fig. 13 The FEA model and one simulation result of the UUV

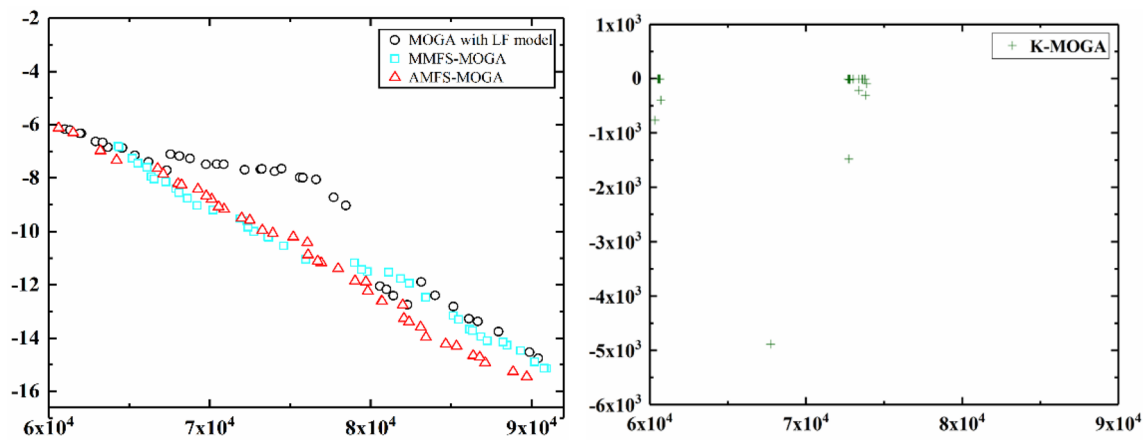


Fig. 14 The typical Pareto frontiers from different approaches for the engineering case

$$\sigma_1 = \frac{k_1 p_j R}{t}, \tag{17}$$

$$\sigma_2 = \frac{k_2 p_j R}{t}, \tag{18}$$

$$\sigma_3 = \frac{k_3 p_j R}{t}, \tag{19}$$

$$P_{E1} = E \left(\frac{t}{R} \right)^2 \left[\frac{0.6}{(u - 0.37)} \right] u \geq 1$$

$$P_{E1} = 1.21 E \left(\frac{t}{R} \right)^2 u \leq 1 \tag{20}$$

$$P_{cr1} = k_4 P_{E1},$$

Table 8 Comparison of MMFS-MOGA and AMFS-MOGA for the engineering case

Metrics	MMFS-MOGA	AMFS-MOGA
RHD	0.1300	0.1231
OS	0.0431	0.0529
FC	90	80

$$P_{E2} = \frac{E}{n^2 - 1 + 0.5\alpha^2} \left[\frac{t}{R} \frac{\alpha^4}{(\alpha^2 + n^2)^2} + \frac{I(n^2 - 1)^2}{R^3 l} \right] \tag{21}$$

$$P_{cr2} = k_5 P_{E2},$$

where $k_1, k_2, k_3, k_4, k_5, u, n, \alpha$ are the coefficients determined by the guide from the China Classification Society (CCS), I is the moment of inertia of the rib.

The finite element analysis (FEA) model is taken as the HF model. It is solved using the ANSYS 18.0 simulation tool. The boundary conditions are listed as: (1) all translation degrees in the right end are fixed; (2) all the translation degrees except the axis degree are fixed in the left end. Meanwhile, the load applying to the outer shell of this structure is equal to 3 MPa, which is used to simulate the pressure under 300 meters' water depth. Beam 188 elements are used to simulate the face panels of the ribs, and Shell 181 elements are used to simulate the shell and the webs of the ribs. The number of the element is more than 30,000 to ensure the simulation results with a desirable accuracy level. The FEA model and one simulation result are shown in Fig. 13.

Since running the HF FEA model is computationally expensive, the proposed AMFS-MOGA approach is used to solve this optimization problem. The setting of NSGA-II in this example is the same as that in ZDT1. The two quality metrics RHD and OS are also used to make comparisons for the Pareto frontiers obtained from different approaches. The $p_{\text{good}} = [1 \times 10^4, -30]$ and $p_{\text{bad}} = [2 \times 10^5, -3]$ are set in the objective function space. Figure 14 depicts the obtained typical Pareto frontiers from four approaches. The X represents the mass and Y represents the global buckling pressure, which are shown in Eq. (16). As observed from Fig. 14, the Pareto frontier from MOGA with LF model is dominated by those from the proposed AMFS-MOGA and MMFS-MOGA. This is expected because relying only on the LF empirical model can result in the unreliable Pareto frontier. It is noted that the K-MOGA cannot obtain a desirable Pareto frontier for this engineering case. A possible reason is that the relationships between the design variables and the objective and constraints are high non-linear, which leads to a distorted kriging surrogate model for the objective functions and constraints under limited HF sample points. Therefore, only the comparison results of the quality of convergence, diversity of Pareto optimum, and the computational efforts for the proposed AMFS-MOGA and MMFS-MOGA are summarized in Table 8. Since direct optimization for this problem is not possible, evaluating the accuracy of the final fronts are implemented by comparing the predicted results with the actual simulation results for the obtained Pareto solutions. The comparison results illustrate that the average relative errors of AMFS-MOGA and MMFS-MOGA for the obtained Pareto solutions are less than 6%, while as observed from Table 8, the proposed AMFS-MOGA can save 12.5% simulation calls over the MMFS-MOGA.

5 Conclusion

In this study, a two-stage adaptive MFS model-assisted MOGA is proposed, in which the information from different fidelity models are integrated to improve the computational

efficiency of MOGA. In the first stage, the fitness values of the individuals are evaluated by the LF model or the LF surrogate model for obtaining a preliminary Pareto frontier. In the second stage, an initial MFS model is constructed based on the data both from the LF model and HF sample points selected from the preliminary Pareto set. Then, this MFS model will be used for the fitness evaluations and adaptively updated according to the developed individual-based updating strategy and generation-based updating strategy. Numerical and engineering cases with different levels of complexities are tested to demonstrate the applicability and efficiency of the proposed AMFS-MOGA approach. The observations are summarized as follows: (1) only relying on a simplified HF model (i.e., LF model) may result in unreliable Pareto frontier, while using a single-fidelity HF model/surrogate model in MOGA is time-consuming or even computationally prohibitive, and (2) the proposed AMFS-MOGA approach can significantly reduce the number of evaluations of the expensive HF model, and at the same time obtain comparable convergence and diversity of the Pareto frontier as those obtained by the MOGA with HF model.

As part of future work, the proposed AMFS-MOGA approach will be further tested on more engineering design problems with higher dimensions. Also, practical engineering design problems always involve uncertainties, extending the AMFS-MOGA approach for addressing the robust optimization problem will also be beneficial to broaden the applicability of the approach.

Acknowledgements This work has been supported by the National Natural Science Foundation of China (NSFC) under Grant No. 51805179 and No. 51775203.

References

1. Kitayama S, Srirat J, Arakawa M, Yamazaki K (2013) Sequential approximate multi-objective optimization using radial basis function network. *Struct Multidiscip Optim* 48:501–515
2. Jiang C, Qiu H, Yang Z, Chen L, Gao L, Li P (2019) A general failure-pursuing sampling framework for surrogate-based reliability analysis. *Reliab Eng Syst Saf* 183:47–59
3. Liu B, Koziel S, Zhang Q (2016) A multi-fidelity surrogate-model-assisted evolutionary algorithm for computationally expensive optimization problems. *J Comput Sci* 12:28–37
4. Roshanian J, Bataleblu AA, Ebrahimi M (2018) A novel evolution control strategy for surrogate-assisted design optimization. *Struct Multidiscip Optim* 58:1255–1273
5. Peng L, Liu L, Long T, Yang W (2014) An efficient truss structure optimization framework based on CAD/CAE integration and sequential radial basis function metamodel. *Struct Multidiscip Optim* 50:329–346
6. Ray T, Smith W (2006) A surrogate assisted parallel multiobjective evolutionary algorithm for robust engineering design. *Eng Optim* 38:997–1011
7. Jin Y (2003) A comprehensive survey of fitness approximation in evolutionary computation. *Soft Comput* 9:3–12

8. Li G, Li M, Azarm S, Rambo J, Joshi Y (2007) Optimizing thermal design of data center cabinets with a new multi-objective genetic algorithm. *Distrib Parallel Databases* 21:167–192
9. Wang H, Jin Y, Jansen JO (2016) Data-driven surrogate-assisted multiobjective evolutionary optimization of a trauma system. *IEEE Trans Evol Comput* 20:939–952
10. Habib A, Singh HK, Ray T (2017) A multiple surrogate assisted evolutionary algorithm for optimization involving iterative solvers. *Eng Optim* 50:1625–1644
11. Pan L, He C, Tian Y, Wang H, Zhang X, Jin Y (2018) A classification based surrogate-assisted evolutionary algorithm for expensive many-objective optimization. *IEEE Trans Evolut Comput* 23:74–88
12. Jin Y, Wang H, Chugh T, Guo D, Miettinen K (2018) Data-driven evolutionary optimization: an overview and case studies. *IEEE Trans Evolut Comput* 23:442–458
13. Sun C, Jin Y, Cheng R, Ding J, Zeng J (2017) Surrogate-assisted cooperative swarm optimization of high-dimensional expensive problems. *IEEE Trans Evol Comput* 21:644–660
14. Dong H, Li C, Song B, Wang P (2018) Multi-surrogate-based differential evolution with multi-start exploration (MDEME) for computationally expensive optimization. *Adv Eng Softw* 123:62–76
15. Wang H, Jin Y, Sun C, Doherty J (2019) Offline Data-driven evolutionary optimization using selective surrogate ensembles. *IEEE Trans Evolut Comput* 23:203–216
16. Jin Y (2011) Surrogate-assisted evolutionary computation: recent advances and future challenges. *Swarm Evolut Comput* 1:61–70
17. Li M (2011) An improved kriging-assisted multi-objective genetic algorithm. *J Mech Des* 133:071008
18. Tian J, Tan Y, Zeng J, Sun C, Jin Y (2018) Multi-objective infill criterion driven gaussian process assisted particle swarm optimization of high-dimensional expensive problems. *IEEE Trans Evolut Comput* 23:459–472
19. Wang H, Jin Y, Sun C, Doherty J (2018) Offline data-driven evolutionary optimization using selective surrogate ensembles. *IEEE Trans Evolut Comput* 23:203–216
20. Yu H, Tan Y, Sun C, Zeng J (2019) A generation-based optimal restart strategy for surrogate-assisted social learning particle swarm optimization. *Knowl Based Syst* 163:14–25
21. Li K, Yu Y, He J, Lin Y (2018) An integrated beam-plate structure multi-level optimal design framework based on bi-directional evolutionary structural optimization and surrogate model. *Adv Eng Softw* 115:230–247
22. Chugh T, Sindhya K, Hakanen J, Miettinen K (2017) A survey on handling computationally expensive multiobjective optimization problems with evolutionary algorithms. *Soft Comput* 23:3137–3166
23. Yu H, Tan Y, Zeng J, Sun C, Jin Y (2018) Surrogate-assisted hierarchical particle swarm optimization. *Inf Sci* 454:59–72
24. Dong H, Song B, Wang P, Dong Z (2018) Hybrid surrogate-based optimization using space reduction (HSOSR) for expensive black-box functions. *Appl Soft Comput* 64:641–655
25. Song X, Lv L, Li J, Sun W, Zhang J (2018) An advanced and robust ensemble surrogate model: extended adaptive hybrid functions. *J Mech Des* 140:041402
26. Li E, Wang H (2016) An alternative adaptive differential evolutionary algorithm assisted by expected improvement criterion and cut-HDMR expansion and its application in time-based sheet forming design. *Adv Eng Softw* 97:96–107
27. Zhang K-S, Han Z-H, Gao Z-J, Wang Y (2019) Constraint aggregation for large number of constraints in wing surrogate-based optimization. *Struct Multidiscip Optim* 59:421–438
28. Han Z, Xu C, Zhang L, Zhang Y, Zhang K, Song W (2019) Efficient aerodynamic shape optimization using variable-fidelity surrogate models and multilevel computational grids. *Chin J Aeronaut*. <https://doi.org/10.1016/j.cja.2019.05.001>
29. Lin Y, He J, Li K (2018) Hull form design optimization of twin-skeg fishing vessel for minimum resistance based on surrogate model. *Adv Eng Softw* 123:38–50
30. Qian J, Yi J, Cheng Y, Liu J, Zhou Q (2019) A sequential constraints updating approach for Kriging surrogate model-assisted engineering optimization design problem. *Eng Comput*. <https://doi.org/10.1007/s00366-019-00745-w>
31. Toal DJJ (2015) A study into the potential of GPUs for the efficient construction and evaluation of Kriging models. *Eng Comput* 32:377–404
32. Bouhlef MA, Martins JRR (2018) Gradient-enhanced kriging for high-dimensional problems. *Eng Comput* 35:157–173
33. Guo Z, Song L, Park C, Li J, Haftka RT (2018) Analysis of dataset selection for multi-fidelity surrogates for a turbine problem. *Struct Multidiscip Optim* 57:2127–2142
34. Park C, Haftka RT, Kim NH (2017) Remarks on multi-fidelity surrogates. *Struct Multidiscip Optim* 55:1029–1050
35. Cai X, Qiu H, Gao L, Shao X (2017) Metamodeling for high dimensional design problems by multi-fidelity simulations. *Struct Multidiscip Optim* 56:151–166
36. Han Z, Zimmerman R, Görtz S (2012) Alternative cokriging method for variable-fidelity surrogate modeling. *AIAA J* 50:1205–1210
37. Liu H, Ong Y-S, Cai J, Wang Y (2018) Cope with diverse data structures in multi-fidelity modeling: a Gaussian process method. *Eng Appl Artif Intell* 67:211–225
38. Xiao M, Zhang G, Breitkopf P, Villon P, Zhang W (2018) Extended co-kriging interpolation method based on multi-fidelity data. *Appl Math Comput* 323:120–131
39. Song X, Lv L, Sun W, Zhang J (2019) A radial basis function-based multi-fidelity surrogate model: exploring correlation between high-fidelity and low-fidelity models. *Struct Multidiscip Optim* 60:965–981
40. Park C, Haftka RT, Kim NH (2018) Low-fidelity scale factor improves Bayesian multi-fidelity prediction by reducing bumpiness of discrepancy function. *Struct Multidiscip Optim* 58:399–414
41. Kennedy MC, O'Hagan A (2000) Predicting the output from a complex computer code when fast approximations are available. *Biometrika* 87:1–13
42. Zhou Q, Wang Y, Choi S-K, Jiang P, Shao X, Hu J et al (2018) A robust optimization approach based on multi-fidelity metamodel. *Struct Multidiscip Optim* 57:775–797
43. Nguyen N-V, Choi S-M, Kim W-S, Lee J-W, Kim S, Neufeld D et al (2013) Multidisciplinary unmanned combat air vehicle system design using multi-fidelity model. *Aerosp Sci Technol* 26:200–210
44. Shu L, Jiang P, Zhou Q, Shao X, Hu J, Meng X (2018) An on-line variable fidelity metamodel assisted multi-objective genetic algorithm for engineering design optimization. *Appl Soft Comput* 66:438–448
45. Liu Y, Collette M (2014) Improving surrogate-assisted variable fidelity multi-objective optimization using a clustering algorithm. *Appl Soft Comput* 24:482–493
46. Zhou Q, Wang Y, Choi S-K, Jiang P (2017) An on-line multi-fidelity metamodel assisted multi-objective genetic algorithm. In: ASME 2017 international design engineering technical conferences and computers and information in engineering conference, Cleveland
47. Deb K, Pratap A, Agarwal S, Meyarivan T (2002) A fast and elitist multiobjective genetic algorithm: NSGA-II. *Evolut Comput IEEE Trans* 6:182–197
48. Zhou Q, Yang Y, Jiang P, Shao X, Cao L, Hu J et al (2017) A multi-fidelity information fusion metamodeling assisted laser

- beam welding process parameter optimization approach. *Adv Eng Softw* 110:85–97
49. Zadeh PM, Toropov VV, Wood AS (2009) Metamodel-based collaborative optimization framework. *Struct Multidiscip Optim* 38:103–115
 50. Zhou Q, Wang Y, Choi SK, Jiang P, Shao X, Hu J (2017) A sequential multi-fidelity metamodeling approach for data regression. *Knowl Based Syst* 134:199–212
 51. Zhou Q, Shao X, Jiang P, Gao Z, Wang C, Shu L (2016) An active learning metamodeling approach by sequentially exploiting difference information from variable-fidelity models. *Adv Eng Inform* 30:283–297
 52. Li M, Li G, Azarm S (2008) A kriging metamodel assisted multi-objective genetic algorithm for design optimization. *J Mech Des* 130:031401
 53. Deb K (2001) *Multi-objective optimization using evolutionary algorithms*. Wiley, Chichester, U.K.
 54. Wu J, Azarm S (2001) Metrics for quality assessment of a multi-objective design optimization solution set. *J Mech Des* 123:18–25
 55. Cheng S, Zhou J, Li M (2015) A new hybrid algorithm for multi-objective robust optimization with interval uncertainty. *J Mech Des* 137:021401
 56. Zhu J, Wang Y-J, Collette M (2014) A multi-objective variable-fidelity optimization method for genetic algorithms. *Eng Optim* 46:521–542

Publisher's Note Springer Nature remains neutral with regard to jurisdictional claims in published maps and institutional affiliations.